Remodeling of lateral geniculate nucleus projections to extrastriate area MT following long-term lesions of striate cortex

Nafiseh Atapour[a,b,1] , Katrina H. Worthy[a], and Marcello G. P. Rosa[a,b]

[a]Neuroscience Program, Biomedicine Discovery Institute and Department of Physiology, Monash University, Clayton, VIC 3800, Australia; and [b]Australian Research Council, Centre of Excellence for Integrative Brain Function, Monash University Node, Clayton, VIC 3800, Australia

Here, we report on a previously unknown form of thalamocortical plasticity observed following lesions of the primary visual area (V1) in marmoset monkeys. In primates, lateral geniculate nucleus (LGN) neurons form parallel pathways to the cortex, which are characterized by the expression of different calcium-binding proteins. LGN projections to the middle temporal (MT) area only originate in the koniocellular layers, where many neurons express calbindin. In contrast, projections to V1 also originate in the magnocellular and parvocellular layers, where neurons express parvalbumin but not calbindin. Our results demonstrate that this specificity is disrupted following long-term (1 to 3 y) unilateral V1 lesions, indicating active rearrangement of the geniculocortical circuit. In lesioned animals, retrograde tracing revealed MT-projecting neurons scattered throughout the lesion projection zone (LPZ, the sector of the LGN that underwent retrograde degeneration following a V1 lesion). Many of the MT-projecting neurons had large cell bodies and were located outside the koniocellular layers. Furthermore, we found that a large percentage of magno- and parvocellular neurons expressed calbindin in addition to the expected parvalbumin expression and that this coexpression was present in many of the MT-projecting neurons within the LPZ. These results demonstrate that V1 lesions trigger neurochemical and structural remodeling of the geniculo-extrastriate pathway, leading to the emergence of nonkoniocellular input to MT. This has potential implications for our understanding of the neurobiological bases of the residual visual abilities that survive V1 lesions, including motion perception and blindsight, and reveals targets for rehabilitation strategies to ameliorate the consequences of cortical blindness.

primate | brain plasticity | striate cortex lesion | extrastriate cortex | blindsight

In primates, damage to the primary visual cortex (V1) leads to scotomas, which are defined by the relationship between the lesion extents and the retinotopic organization of this area (1). These lesions also trigger degenerative changes in the lateral geniculate nucleus (LGN) of the thalamus, which is the critical link between the retina and V1. Over several months, the majority of neurons in the affected sector of the LGN (lesion projection zone, LPZ) undergo retrograde degeneration leading to a marked reduction in the volume of this nucleus (2–5). However, a surviving population of LGN neurons retains visual function, including receptive fields inside the scotomas (6). At least some of these neurons receive retinal inputs (7) and form direct projections to extrastriate areas (3, 8, 9). This evidence is compatible with the hypothesis that surviving neurons within the LPZs provide one of the pathways for the mediation of residual visual function within the scotomas [blindsight (10)], as also indicated by functional studies in human and nonhuman primates (11–13).

Although degenerative changes in the LGN are well documented, the possibility of other forms of plasticity following V1 lesions has not been investigated. Here, we address two interrelated aspects of this question, with a focus on LGN projection

neurons: changes in connections with the middle temporal area (MT) and in the expression of calcium-binding proteins. Area MT is central for the processing of direction and speed of motion (14–16) and is one of the extrastriate areas most often linked to residual vision and blindsight (17–19). In the normal simian brain, projections from the LGN to MT are formed by neurons in the koniocellular (K) layer, of which many express the calcium-binding protein calbindin-D28k (CB) (20–23). In contrast, projection neurons in the magnocellular (M) and parvocellular (P) layers, which are not thought to target MT, express the calcium-binding protein parvalbumin (PV) (21, 22). Currently, it is believed that any contributions of the LGN-MT pathway to blindsight and residual vision are likely to rely on projections of surviving K-layer neurons (11, 17, 23–25).

Our experiments, involving retrograde tracing of the projections from the LGN to MT in both normal and V1-lesioned marmosets (*Callithrix jacchus*), led to two unexpected observations. First, following long survival times (>1 y), neurons projecting to MT were found across the entire extent of the LPZ, including beyond the K layers. Second, most neurons in the M and P layers of the LGN show CB expression in addition to the expected PV expression, and many of the MT-projecting neurons show this pattern of coexpression, compatible with the hypothesis that they are surviving M and/or P neurons. These results indicate that primate V1 lesions lead to a previously unknown form of thalamocortical plasticity. This rearrangement of the geniculo-extrastriate pathway could underlie some aspects of recovery of function in the aftermath of V1 lesions,

Significance

Lesions of the primary visual area (V1) in primates cause blindness by severing the main pathway which brings information from the thalamus to the cortex. However, some visual abilities remain, which are hypothesized to be mediated by thalamic neurons that innervate surviving areas such as the middle temporal (MT) cortex. We found that V1 lesions trigger long-term plasticity in the connections between the thalamus and cortex, including the emergence of a pathway that brings information to MT from cell populations that would normally project to V1. These results reveal potential targets for rehabilitation strategies to ameliorate the consequences of cortical blindness.

NEUROSCIENCE

including mediating preservation of visual responses in MT (26, 27), and contribute to rehabilitation therapies for motion perception (19, 28).

Results

Projections to Area MT. In animals with long-term V1 lesions, the LGN showed a clear demarcation between the LPZ, where neuronal density was markedly reduced, and regions where the normal histological appearance of this nucleus was preserved (Fig. 1). As expected from the extent of the lesions (see *Materials and Methods*), the LPZs occupied the caudal pole of the LGN and the representation of the peripheral horizontal meridian, leading to wedge-shaped sectors of degeneration visible in coronal sections through the center of this nucleus. Animals with lesions incurred in early postnatal life (6 wk from birth) and in young adulthood were similar in this respect (Fig. 1). Large numbers of astrocytes were also observed around neurons in the LPZ (*SI Appendix*, Fig. S1) as previously reported in the macaque (29).

Following injections of fluorescent tracers (fast blue and diamidino yellow; FB and DY) in area MT of both neonatal- and adult-lesioned animals (*SI Appendix*, Fig. S2), we found that the LPZ contained a concentration of retrogradely labeled neurons, which were scattered throughout its dorsoventral extent (Figs. 1 and 2 *A–L*). Many of these cells had large, brightly labeled somata, which could be discerned even at low power (Fig. 1). The correlation of MT-projecting cells with the LPZ was striking; non-LPZ tissue showed much fewer labeled cells, which were mostly located close to the boundary with the LPZ or within a K layer (Figs. 1 and 2). MT-projecting neurons displayed a wide variety of sizes (10 to 40 μm) and morphologies (Fig. 2, *Bottom*).

The pattern of MT projections in lesioned animals contrasted with that observed in control (nonlesioned) animals. Consistent with previous observations in the marmoset (9, 30) and other primates (23, 31, 32), in these cases, tracer injections in MT led to sparsely distributed labeled neurons in the LGN, which were restricted to the K1 and K3 layers (33). This distribution is
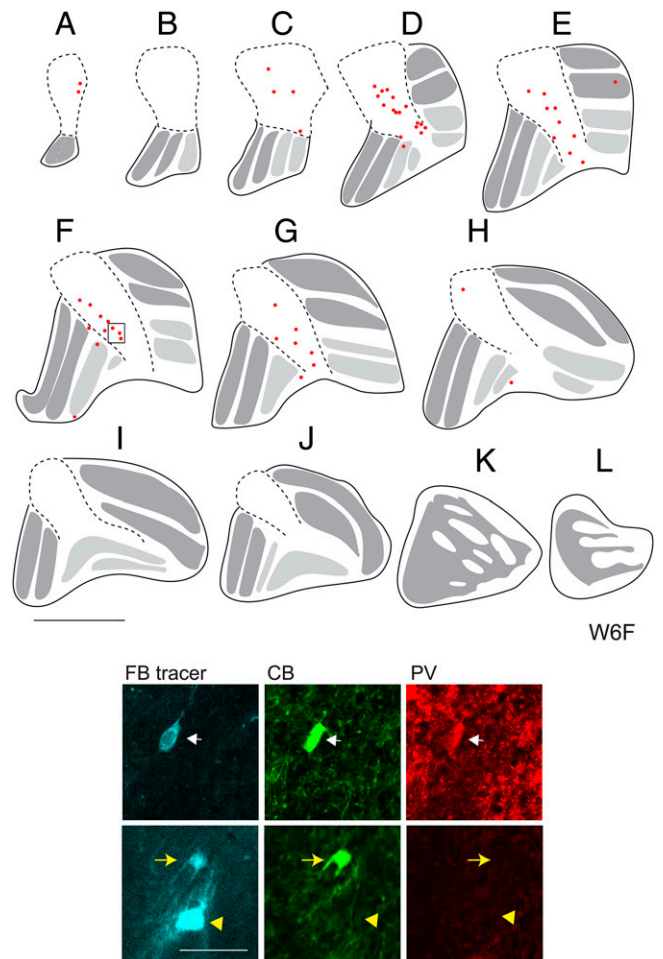

Fig. 2. Localization and neurochemistry of MT-projecting LGN neurons in an animal with V1 lesions. *A–L* are drawings of equally spaced coronal sections spanning from the caudal (*A*) to the rostral (*L*) poles of the LGN in case W6F. (Scale bar, 1 mm.) In these drawings, dotted lines designate the approximate borders of the LPZ, dark and light gray indicate parvo- and magnocellular layers outside the LPZ, and red circles show the locations of neurons retrogradely labeled with FB. MT-projecting neurons collectively span the entire dorsoventral extent of the LPZ. (*Bottom*) Confocal images of neurons sampled from *F* (boxed area) showing the tracer FB and immunoreactivity to CB and PV. White arrows point to a neuron expressing both CB and PV; yellow arrows point to a neuron expressing CB only, and yellow arrowheads point to a neuron with no immunoreactivity to either CB or PV. (Scale bar, 50 μm.)
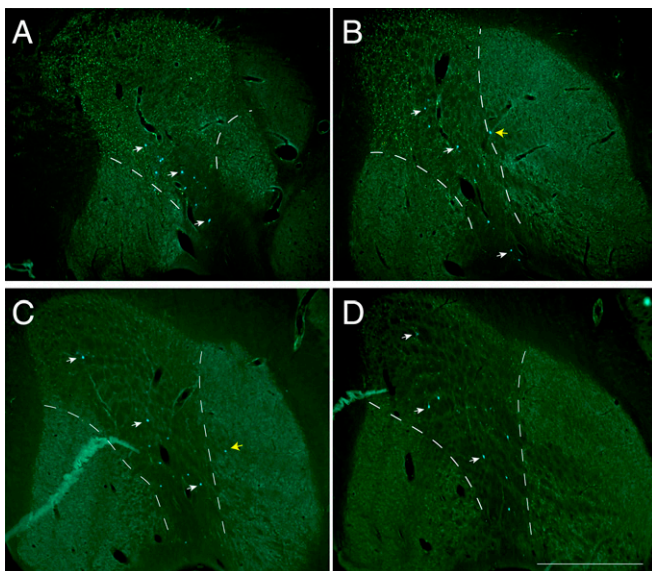
exemplified in Fig. 3 *A–L* (CJ207, a case which yielded one of the largest numbers of labeled cells in the LGN). MT-projecting neurons in nonlesioned animals were small, with the vast majority having cell bodies 10 to 20 μm in diameter (Fig. 3, *Bottom*).

Neurochemical Changes in the LGN. Given that neurons in the K layers are traditionally thought to have neurochemical signatures that are distinct from those in the M and P layers, we sought to establish the identity of LPZ MT-projecting cells by establishing their immunoreactivity for calbindin and parvalbumin. This led to a second unexpected observation: whereas in normal animals, the well-described specificity was confirmed (M and P neurons expressing parvalbumin, K neurons expressing either calbindin, or neither calcium-binding protein), in animals with long-term V1 lesions a large proportion of P and M neurons expressed both parvalbumin and calbindin (Fig. 4 and *SI Appendix*, Fig. S3). Furthermore, as described later, we found that many of the MT-projecting cells in the LPZ showed this pattern of coexpression, indicating that they are M or P neurons.

Fig. 1. Neurons retrogradely labeled by tracer injection in area MT concentrate in the LPZ. Each panel shows a low-power view of a coronal section through the marmoset LGN. (Scale bar, 500 μm.) (*A* and *B*) Adult lesion case (WA18). (*C* and *D*) Case with lesion incurred at 6 wk of age (W6I). The dashed lines indicate the borders of the LPZs, where the majority of neurons had undergone retrograde degeneration (4). In all panels, large FB-labeled neurons are visible, which collectively span the dorsoventral axis of LGN within the degenerated area. White and yellow arrows point to examples of MT-projecting neurons within and outside the LPZ, respectively.
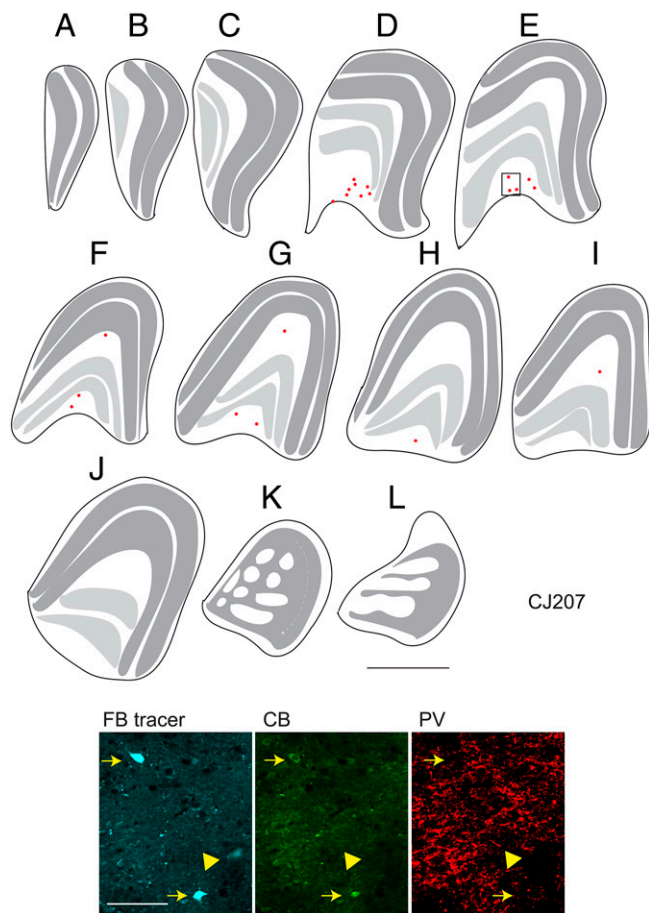
Fig. 3. Localization and neurochemistry of MT-projecting neurons in the LGN of a nonlesioned animal. *A–L* are drawings of equally spaced coronal sections spanning from the caudal (*A*) to the rostral (*L*) poles of the LGN in case CJ207. (Scale bar, 1 mm.) Conventions as in Fig. 2. All MT-projecting neurons are localized within K layers. (*Bottom*) Confocal images of neurons sampled from *E* (boxed area) showing the tracer FB and immunoreactivity to CB and PV. Yellow arrows point to neurons expressing only CB and the yellow arrowheads to a neuron with no immunopositivity to either CB or PV. (Scale bar, 100 μm.)

Immunofluorescence staining of LGN sections for CB and PV in nonlesioned animals revealed the expected neurochemical characteristics of M, P, and K layers (Fig. 4, *Top*), based on previous studies in both marmoset and macaque monkeys (22, 23, 34). A population of neurons in the K layers expressed CB, while neurons in the M and P layers expressed PV; coexpression of CB and PV was minimal or absent (Fig. 4, *Top* and Fig. 5*A*, control [CON] cases).

In contrast, in V1-lesioned cases, we found that substantial numbers of LGN neurons, even outside the LPZs, coexpressed CB and PV (Fig. 4, *Bottom* and *SI Appendix*, Fig. S3). This coexpression was observed in both the M and P layers and occurred not only in the nondegenerated part of the ipsilesional LGN but also in the contralesional LGN (Fig. 5*A*; note that contralesional LGN data were not available for case WA11). K neurons remained positive for CB only. The population of CB-expressing K neurons remained segregated from that of neurons coexpressing both CB and PV in the M and P layers (Fig. 6*A*).

Quantitative analysis suggested that CB expression in the M and P layers contralateral to the lesion was achieved gradually, within a timescale of months to years. In most cases, the percentage of CB-expressing M and P neurons was higher in the ipsilesional LGN than in the contralesional LGN (Fig. 5*A*).

The single exception was the animal with the longest postlesion survival time (WA9; >3 y), in which the percentage of coexpressing neurons was similar in both hemispheres. The percentage of CB-expressing neurons in the M layers of the contralesional LGN was positively correlated with the postlesion survival time, although it did not reach to a significant level (Fig. 5*D*, $r^2 = 0.6$, $P = 0.12$). In the P layers, CB expression was evident in the ipsilesional LGN in some cases but not all. Overall, the ratio of contralesional/ipsilesional CB expression among M and P neurons was strongly correlated with postlesion survival time (Fig. 5*E*, $r^2 = 0.97$, $P < 0.01$). In comparison, the size of the effective V1 lesion, estimated by the volume reduction in LGN relative to the contralesional hemisphere, appeared not to be as strong a determining factor in the degree of CB expression in M and P neurons (*SI Appendix*, Fig. S4).

Statistical comparison of the average percentages of CB-expressing M and P neurons in neonatal and adult lesion cases showed no significant difference in either hemisphere [Fig. 5*B*, two-way ANOVA; interaction, F (1, 7) = 1.33, P = 0.28;
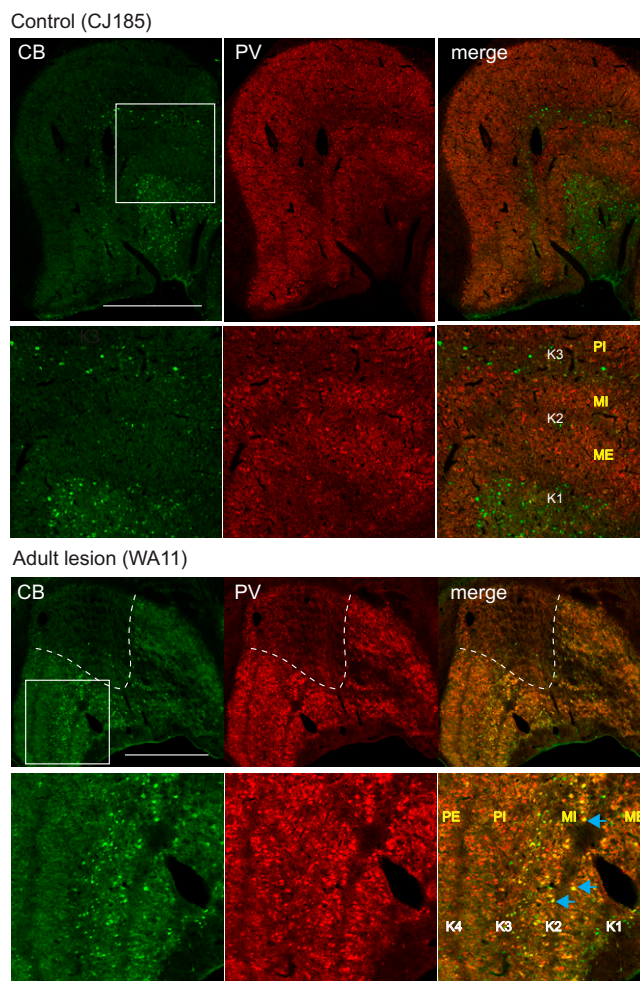

Fig. 4. Unexpected expression of CB in the M and P layers of the LGN. (*Top*) LGN of a normal adult animal (CJ185). (*Bottom*) LGN of an animal (WA11) with V1 lesion in adulthood, with the dashed line indicating the LPZ. In both cases, the boxed area in the CB-stained images (*Left*) are shown in higher magnification. In the bottom row, blue arrows point to examples of M neurons with colocalized expression of CB and PV, which are only visible in lesioned cases. Other abbreviations: K1 through K4: koniocellular layers; ME: magnocellular external layer; MI: magnocellular internal layer; PE: parvocellular external layer; PI: parvocellular internal layer. (Scale bar, 1 mm.)
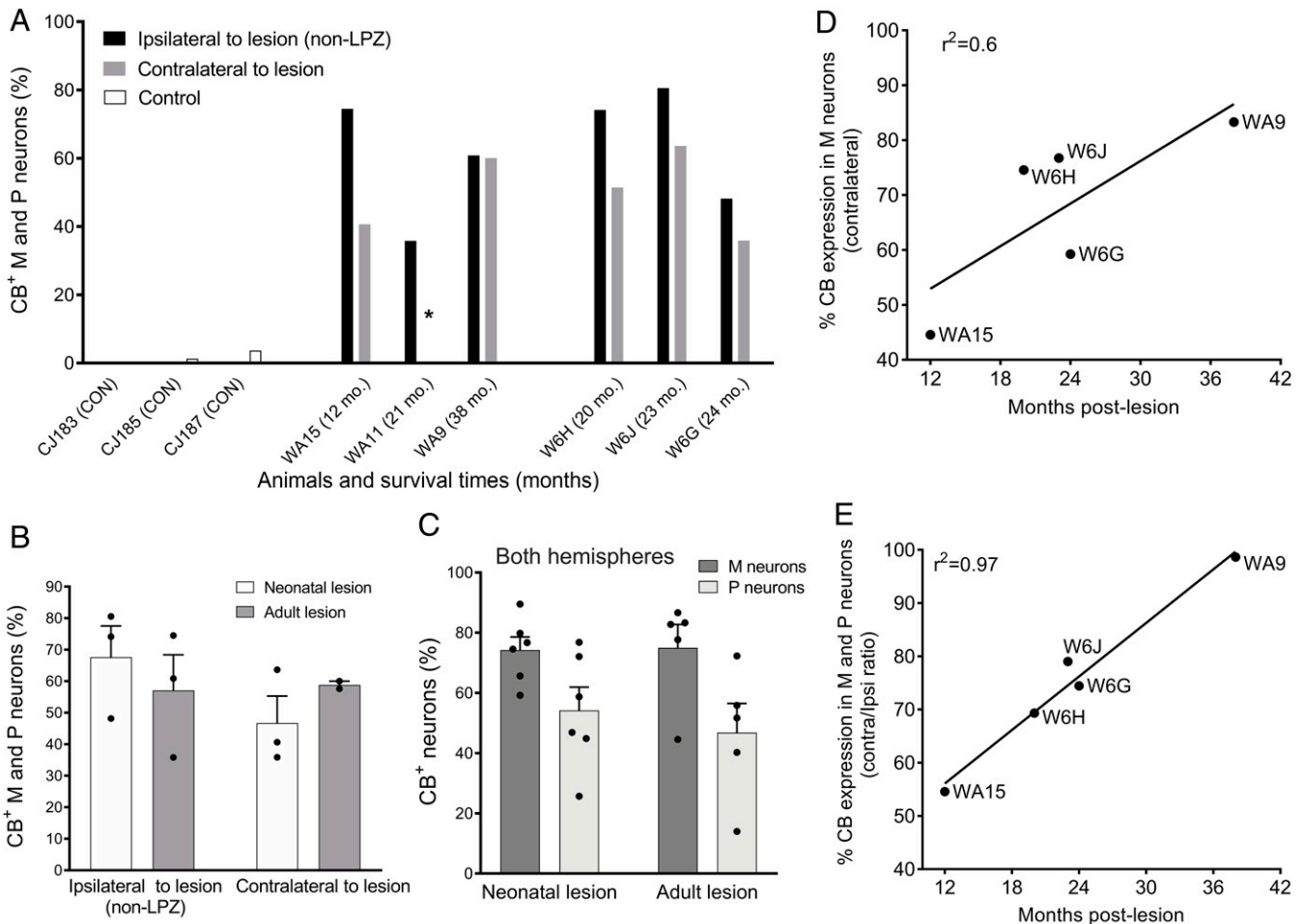
Atapour et al.
Remodeling of lateral geniculate nucleus projections to extrastriate area MT following long-term lesions of striate cortex

PNAS | 3 of 10
https://doi.org/10.1073/pnas.2117137119

Fig. 5. Quantification of CB expression in the LGN following V1 lesions. Data obtained from the LGN ipsilateral to the lesion are from regions outside the LPZ. All quantification is based on three animals with best staining in each group. (*A*) Percentage of CB$^+$ (CB-expressing) M and P neurons in the LGN for each animal. In control animals (CON), only one LGN was evaluated. The asterisk indicates unavailability of data from the LGN contralateral to the lesion in case WA11. (*B*) Mean ± SEM percentage of CB-expressing M and P neurons in the LGN of V1-lesioned animals. (*C*) Data from both hemispheres (in *B*) are pooled to indicate coexpression in M and P neurons separately. In *B* and *C*, individual points show the mean of data for each animal across multiple sections. (*D*) Percentage CB expression in the M neurons of contralateral LGN as a function of postlesion survival. (*E*) Ratio of the percentages of CB-expression in M and P neurons in the LGNs contralateral and ipsilateral to the lesion as a function of postlesion survival.

hemisphere, F (1, 7) = 0.95, P = 0.36, lesion age, F (1, 7) = 0.006, P = 0.94]. The proportion of CB-expressing neurons tended to be higher in the M layers compared to P layers in both ipsilateral and contralateral hemispheres. However, an analysis pooling data from both hemispheres (Fig. 5*C*) showed that the difference was not statistically significant, likely reflecting variability among cases [two-way ANOVA; interaction, F (1, 18) = 0.29, P = 0.59; hemisphere, F (1, 18) = 0.19, P = 0.66; lesion age, F (1, 18) = 10.48, P = 0.004, Tukey's test for all possible comparisons, P > 0.05].

Within the LPZs, we consistently observed neurons coexpressing CB and PV at levels corresponding to the degenerated M and P layers. These neurons were observed in addition to those that only expressed CB, with these two populations often intermingled near the laminar boundaries (Fig. 6*A*). Approximately half of the CB-expressing neurons in the LPZs coexpressed PV, with no difference being apparent between neonatal (50.9 ± 7.1%) and adult (47.0 ± 6.6%) lesioned groups (P = 0.7, Fig. 6*B*). However, the percentage of CB-expressing surviving neurons within the LPZs (relative to all surviving neurons, based on neuronal nuclei [NeuN] staining) was significantly higher in the neonatal lesion group compared to the adult lesion group (51.9 ± 8.1 versus 16.7 ± 1.6, P = 0.01, Fig. 6*C*).

Neurochemical Identity of MT-Projecting Neurons in the LPZ. Based on the expression of calcium-binding proteins in the M and P layers outside the LPZs, we identified MT-projecting neurons that coexpressed CB and PV as putative M or P neurons. Supporting this finding, we located coexpressing MT-projecting neurons in regions that could unambiguously be assigned to an M layer (Fig. 7). Many of these neurons had the expected morphological characteristics of M neurons (i.e., nucleus boundaries were clear within the large cell and expression of PV was limited to the cytoplasm; Fig. 7, *Top*). Most of the CB- and PV-coexpressing neurons were located well within the LPZ or in close proximity of the LPZ (Fig. 7, *Top* and *Middle*). However, we also found examples of isolated cells in what would be expected to be parts of the LGN not directly affected by the V1 lesion (Fig. 7, *Bottom*).

CB- and PV-coexpressing neurons comprised, on average, 34.9 ± 6.4% and 36.2 ± 3.6% of the labeled MT-projecting neurons in neonatal and adult lesion groups, respectively (Fig. 8 *A* and *B*). In Fig. 8*C*, we present the number of labeled neurons in the LGN normalized relative to the number of labeled neurons found in a nonvisual structure (the intralaminar thalamic nuclei) to mitigate the likely effect of variation in the extent of the effective injection sites. Although there was a trend toward
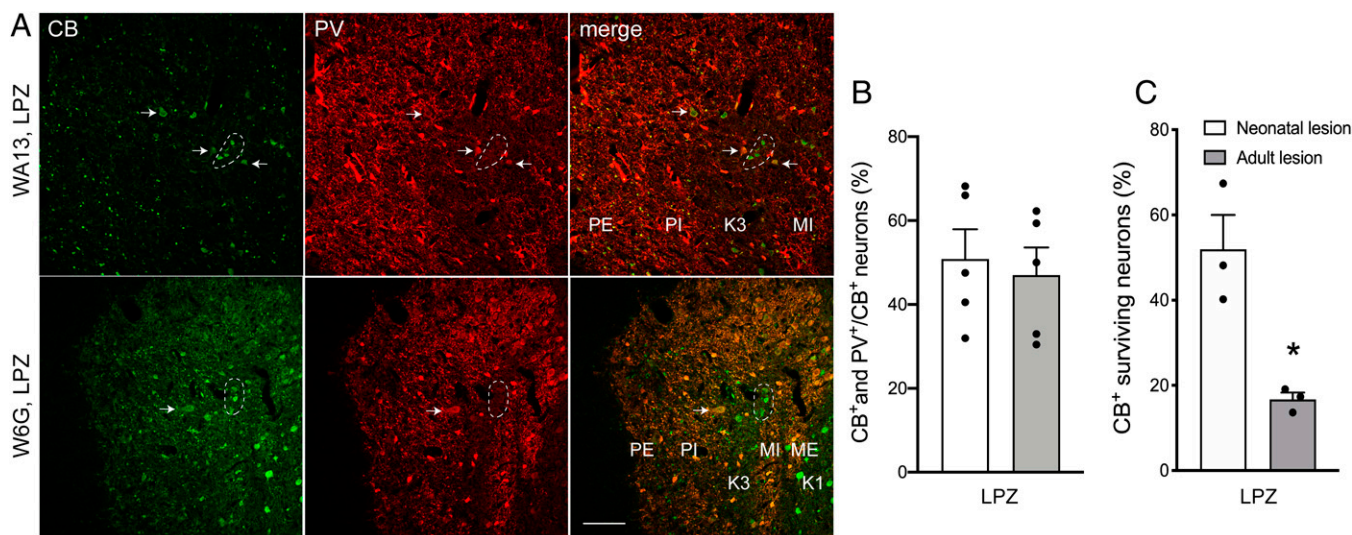
Fig. 6. Coexpression of CB and PV in surviving LGN neurons of the LPZ. (*A*) Immunostaining for CB and PV in WA13 (adult lesion) and W6G (neonatal lesion). White dashed borders highlight neurons expressing only CB, fitting to the K neurons. Arrows point to examples of surviving neurons coexpressing CB and PV, which are putative M and P neurons. Layer abbreviations are as in Fig. 4. (Scale bar, 100 μm.) (*B*) Percentage of neurons coexpressing CB and PV (CB$^+$/PV$^+$) among the population of CB-expressing (CB$^+$) neurons in the LPZ. (*C*) CB$^+$ neurons in the LPZ expressed as percentage of all surviving neurons labeled by NeuN. In *B* and *C*, individual points show the mean of data across several sections for each animal. Mean ± SEM; *P < 0.05.

larger numbers of labeled cells in lesioned cases, the variability of injection effectiveness resulted in no significant difference [one-way ANOVA; F (2, 11) = 0.12, P = 0.88]. Among the lesioned cases, the number of tracer-labeled neurons in the LGN was not significantly correlated with V1 lesion size (Fig. 8*D*, $r^2 = 0.32$, P = 0.08).

Tracer-labeled neurons were also present in the remaining part of V1, extending all the way to the boundaries of the lesion. As shown in *SI Appendix*, Fig. S5, the vast majority of these cells were located in the lower end of layer 3, also known as Brodmann's layer 4B (35), with only isolated labeled cells in layer 6. This pattern is identical to that observed in normal animals (36).

Discussion

Given that the normal LGN projection to area MT is formed by K-layer neurons (23, 30, 32), it has been assumed that any possible contribution of the LGN-MT pathway to visual function after V1 lesions depends on this population. The present results challenge this interpretation by providing evidence that, following long survival times, projections to area MT also originate from neurons located in other LGN layers. This indicates that V1 lesions trigger structural plasticity in the geniculo-extrastriate projection. Thus, it is possible that residual visual abilities within scotomas, including certain forms of blindsight (10) and conscious motion perception (37), also rely on information channeled through surviving neurons in the M and P layers. Given that the present study addressed the spontaneous remodeling of the geniculocortical projection (i.e., under the animal's usual visual environment; see *Materials and Methods*), no behavioral data that could clarify the nature and extent of residual vision in these animals were obtained. Thus, an interesting future direction will be to test if rehabilitation programs (19) have an impact on visual thalamocortical projections including those from the LGN.

The claim of plasticity involving the M (and possibly P) layers is based on three findings. First, many of the MT-projecting neurons display a neurochemical profile (CB and PV coexpression) that is associated with M and P cells following long-term V1 lesions. These neurons are absent or extremely rare in nonlesioned animals but become numerous in the aftermath of V1 lesions. Second, MT-projecting cells are present throughout a radial column that encompasses the entire laminar extent of the LPZ, whereas in normal animals, they are well restricted to the K layers. Third, many of these cells have large cell bodies, which can be visualized even at relatively low magnification (Fig. 1), and other morphological characteristics of M, and possibly P, neurons. Overall, this evidence cannot be parsimoniously interpreted in light of a model whereby this projection is formed exclusively by K neurons. However, it should be remembered that "typical" MT-projecting K neurons, with small cell bodies and expressing only CB or neither calcium-binding protein, still exist in the expected locations of the K layers. Coexpression of CB and PV in M neurons has not been reported in the normal simian LGN, although this possibility has been discussed in a study of the prosimian *Galago* (38).

Multiple lines of evidence have pointed to the likely involvement of the pathway through the superior colliculus and pulvinar in residual vision following V1 lesions (17, 39–43), but the importance of surviving LGN neurons has only started to be recognized recently (12, 13). The present results help clarify the range of mechanisms by which the LGN may play this role, showing that its connections to area MT rely not only on the survival of K-layer neurons but also on plasticity affecting M- (and possibly P-) layer neurons.

CB Expression in M and P Neurons Following V1 Lesion. One key finding of the present study is the clear change in the neurochemical profile of M and P neurons following V1 lesions, which hint at biochemical processes triggered by the loss of target neuronal populations and/or corticogeniculate feedback (5). We provide evidence that this change occurs gradually, with longer survival times leading to larger percentages of PV- and CB-coexpressing neurons. Intriguingly, these changes also involve the LGN contralateral to the lesion, albeit in a delayed manner, implying larger-scale network changes (Fig. 5). Lesion-induced plasticity in the contralesional hemisphere has been observed in both the visual and other sensory systems (44, 45).

The CB expression in M and P neurons after V1 lesion is likely to be part of a response to injury. CB has an anti-apoptotic effect mediated primarily by its ability to directly inhibit caspase-3 activity (46) and can protect cells against excitotoxic damage in monkeys and in patients with Parkinson's disease (47–49). The
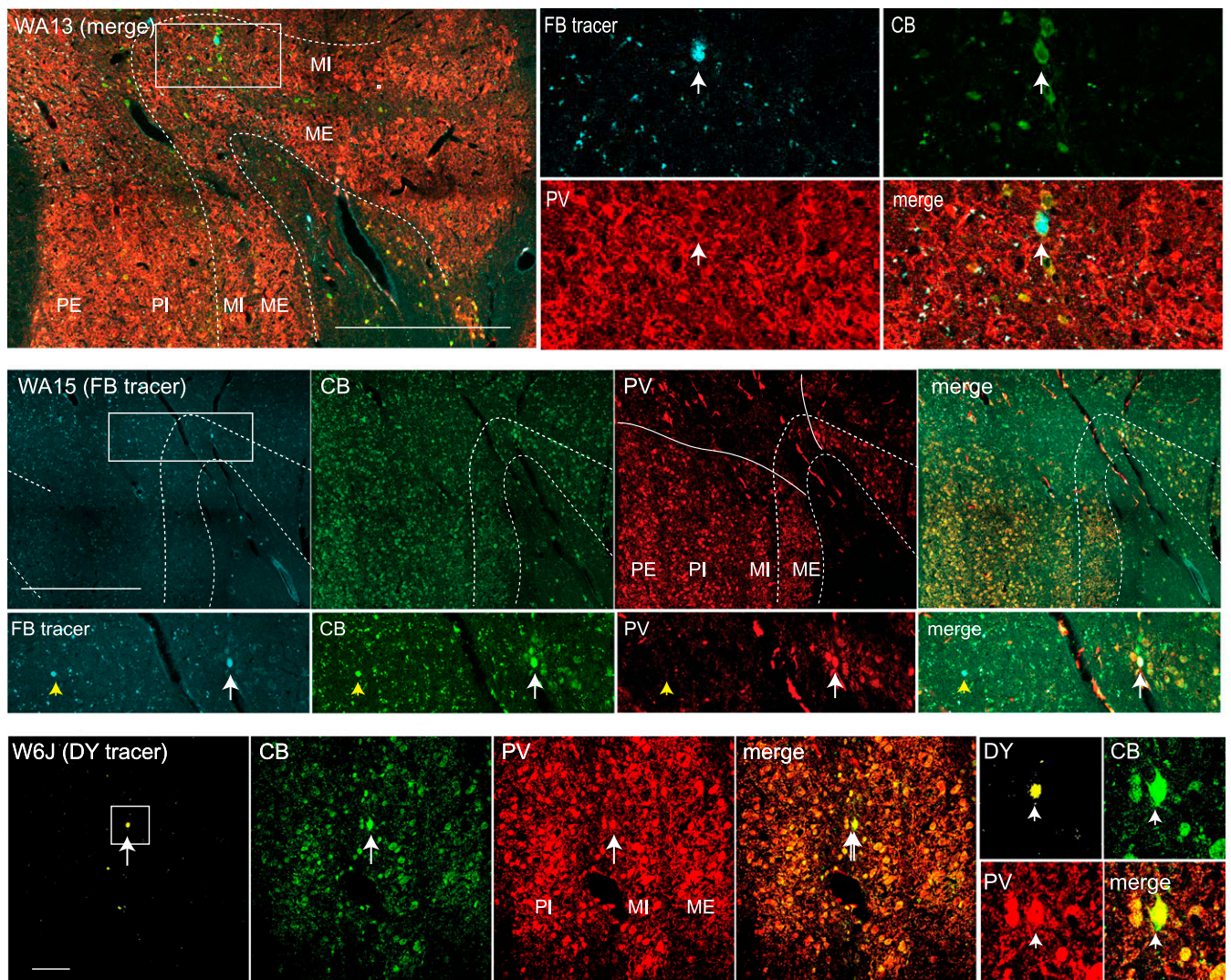
NEUROSCIENCE

Fig. 7. Magnocellular neurons project to the area MT following V1 lesions. Confocal images of parts of LGN containing tracer-labeled neurons located within M layers in two adult lesion cases (*Top*: WA13, *Middle*: WA15) and one neonatal lesion case (*Bottom*: W6J). Three representative neurons, shown in higher magnification, coexpress CB and PV. (*Top*) An FB-traced neuron located within the magnocellular internal (MI) layer. (*Middle*) An FB-traced neuron located within the magnocellular external (ME) layer. (*Bottom*) A DY-labeled neuron within the MI layer. (Scale bars, *Top* and *Middle*, 0.5 mm; *Bottom*, 100 μm.) Layer abbreviations are as in Fig. 4.

removal of CB from a transgenic mouse model of Alzheimer's disease aggravates pathogenesis (50), and its overexpression in hippocampal progenitor cells increases neuronal differentiation and neurite outgrowth (51). Conversely, monocular enucleation leads to a decrease in the density of CB-expressing neurons in the rat LGN (52), supporting the idea that retinal activity is a driver of CB expression. Thus, reduction of cortical feedback following lesions could lead to imbalanced retinal activation of LGN projection neurons, triggering increased CB expression. Consistent with this hypothesis, receptive fields of surviving LGN neurons are reported to be larger than normal, particularly in the M layers (6). Moreover, retinal degeneration largely spares ganglion cells projecting to M neurons, where the CB overexpression is the most significant (53–56).

Contribution of PV-Expressing Neurons to the LGN-MT Pathway in V1-Lesioned Animals. PV-expressing neurons formed approximately one-third of the projections from LGN to MT, both in neonatal and adult V1 lesion cases. Some of the PV-expressing MT-projecting neurons were clearly located in the M layers (Fig. 7) and had the morphological features expected from

M neurons. The more dominant CB expression in M neurons, in comparison with P neurons, is in line with the fact that the dominant source of visual input to MT is via V1 layers associated with the M pathway and the role of M neurons in motion detection (15, 57). However, multisynaptic pathways from V1 to MT also provide P input (31). While we could not unambiguously determine that P neurons project to MT, we did observe neurons coexpressing PV and CB within the degenerated P layers (Fig. 6A).

Lesions in Early Postnatal Life versus Adulthood. It has been shown previously that early postnatal lesions are associated with greater preservation of the direct retinal input to the inferior pulvinar nucleus, which is normally pruned in early postnatal life (9). Since inferior pulvinar neurons also project to area MT (30), it has been proposed that this pathway enables better visual function outcomes in primates with neonatal lesions in comparison with adult lesions. Although our study also incorporated neonatal and adult lesions of V1, we found no quantitative difference in the connectivity of M/P neurons between animals in these groups, suggesting that the different visual pathways to extrastriate cortex are subject to different mechanisms of plasticity. The formation and pruning
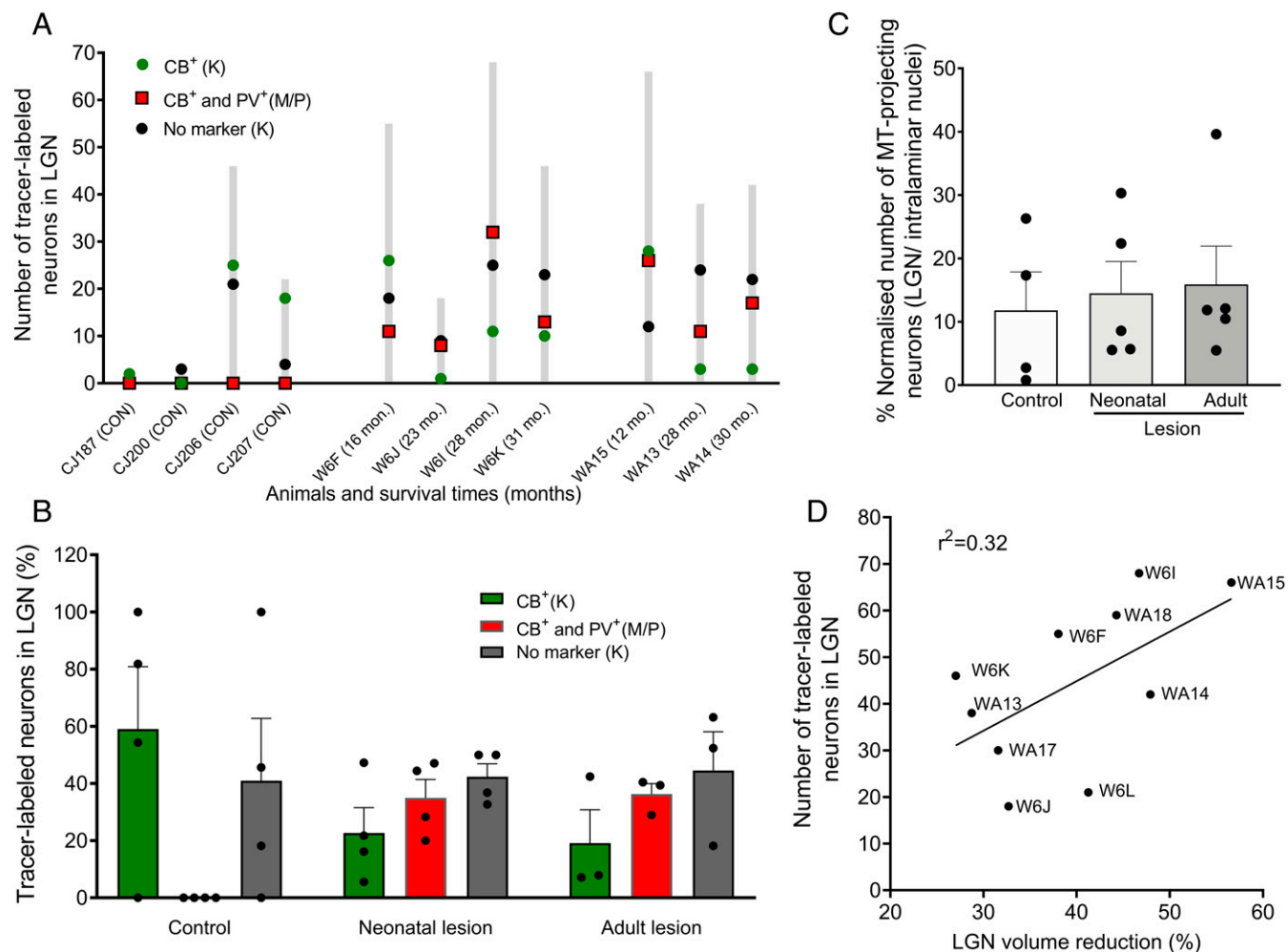
Atapour et al.
Remodeling of lateral geniculate nucleus projections to extrastriate area MT
following long-term lesions of striate cortex

Fig. 8. Quantification of MT-projecting neurons in the LGN following V1 lesions. (*A*) Number and neurochemical identity of MT-projecting neurons in the LGN of different animals. (*B*) Mean ± SEM of the percentages of MT-projecting neurons in the LGN of control, neonatal V1 lesion, and adult V1 lesion animals classified as CB-only expressing (CB$^+$), CB and PV coexpressing (CB$^+$ and PV$^+$), or those expressing neither protein. (*C*) Mean ± SEM of the number of MT-projecting neurons in the LGN of control and lesioned animals, normalized as the percentage of the number of tracer-labeled neurons in the thalamic intralaminar nuclei. (*D*) Correlation between the number of MT-projecting neurons in LGN and V1 lesion size (estimated by the reduction in the volume of the ipsilesional LGN relative to the contralesional LGN).

of retinal projections to different layers of the primate LGN occur prenatally (58), creating fewer opportunities to preserve alternative inputs following postnatal lesions. Moreover, in contrast with the LGN, V1 lesions in either early postnatal or adult life do not result in retrograde degeneration of neurons in the pulvinar complex (59). However, our adoption of very long survival times did not allow for testing differences in the rate of formation of direct M/P connectivity to MT in the two age groups, which may be addressed by future studies.

Even though there was no apparent difference in connections with MT, the results also indicate more significant numbers of CB-expressing neurons in the LPZ of animals with early postnatal lesions compared to adults. Studies in adult macaque monkeys (39) indicate that some K neurons may also undergo retrograde degeneration following V1 lesions. The higher number of CB-expressing neurons may hint at better survival of these neurons in the neonatal lesion group, which can have consequences for the overall visual function.

Possible Mechanisms of Plasticity. The present evidence of monosynaptic projections of M and P neurons to area MT raises the question of what type of structural plasticity could be involved in the aftermath of V1 lesions. One plausible model would be the

unmasking of collaterals of projection neurons which are metabolically inactive in normal animals and thus not readily detectable by retrograde tracers until the destruction of the major branch (3). A second, not mutually exclusive scenario would be based on sprouting and growth of axons of M and P neurons toward MT. Projections from P- and M-layer neurons to area V4 have been reported, although this result needs to be considered with caution, since it predates the recognition of the K pathway as a distinct geniculocortical channel (8). Assuming that V4 normally receives sparse projections from these layers, the amount of sprouting required by this mechanism would be within the range reported in the adult squirrel monkey premotor cortex following cortical lesions (60) and in cat V1 following retinal lesions (61). In addition, axonal branching in M and P neurons that target the remaining parts of V1 could contribute to this process, in particular explaining why we observed M cells projecting to MT outside the LPZs (Fig. 7). The loss of structural integrity in the extracellular matrix following lesions (62, 63) may facilitate neurite growth and tracer pickup by initially inactive axonal branches. Finally, evidence of gamma-aminobutyric acid (GABA) (5) and CB expression in M/P neurons supports trophic neurite outgrowth within the LGN (64), which could explain the increased receptive field sizes of M neurons in the LPZ (6).

In summary, we provide evidence of a structural rewiring in the primate visual thalamo-cortical circuitry after long-term V1 lesions, both in infancy and adulthood. This plasticity brings about an additional route linking the LGN to MT, which may help explain part of the role of LGN in residual vision. The protracted nature of the biochemical changes we document suggests that visual function linked to the M and P pathways may develop gradually over the months or years following V1 lesions, providing a hypothesis for future behavioral studies in both human and nonhuman primates.

Materials and Methods

Animals. Details regarding animals used in this study and their treatments are summarized in Table 1. A total of 20 marmoset monkeys (*C jacchus*) were used in this study. Some of the animals were used for other experiments but had brain tissue acquired for the present purposes. A total of 14 of these animals received lesions of V1 either at 6 wk of age (neonatal lesion) or in adulthood (adult lesion), and 14 animals (including four adult controls, five with neonatal lesions, and five with adult lesions) received injections of fluorescent tracers in area MT. The experiments were conducted in accordance with the Australian Code of Practice for the Care and Use of Animals for Scientific Purposes. All procedures were approved by the Monash University Animal Ethics Experimentation Committee, which also monitored the health and well-being of the animals throughout the experiments.

V1 Lesions. The procedure for V1 lesions was similar to that used in previous studies (4, 6, 27), with slight refinements incorporated into the drug administration protocol. The day before surgery, animals were premedicated with oral meloxicam (Metacam; Boehringer Ingelheim, 0.01 mg/kg [neonates] or 0.1 mg/kg [adults]) and cephalexin (Ibilex; Alphapharm P/L, 30 mg/kg). On the day of the surgery, an intramuscular (i.m.) injection of atropine (Atrosite; Ilium, 0.2 mg/kg) was administered as premedication (adult animals only) 30 min prior to the induction of anesthesia with 2 to 5% isoflurane (Isorrane; Baxter) in oxygen. Dexamethasone (Dexason; Ilium, 0.3 mg/kg, i.m.) was also administered before the animals were positioned in a modified stereotaxic head holder. Body temperature, heart rate, and blood oxygenation (PO_2) were continually monitored, and the rate of anesthetic was continuously adjusted (isoflurane 2 to 5%) to maintain areflexia, relaxed breathing, and low heart rates. Under sterile conditions, a craniotomy was made over the occipital pole of the left hemisphere. Using a fine-tipped cautery, an excision was then made of all cortical tissue caudal to a plane extending from the dorsal surface of the occipital lobe to the cerebellar tentorium, across its entire mediolateral extent (65). This type of lesion removes the central visual field

representation in the occipital operculum as well as of the peripheral representation (in the calcarine sulcus) up to a minimum of 40° eccentricity along the horizontal meridian (5, 66). This corresponds to a minimum of 70% of the unilateral extent of V1 while sparing the majority of secondary visual area (V2) except for the border region with V1 in the central representation, as determined by electrophysiology (6). After application of hemostatic microspheres (Arista AH; BARD Davol Inc.), the surfaces of the exposed occipital cortex and tentorium were protected with ophthalmic film (Gelfilm; Pfizer Inc.), and the cavity was filled with Gelfoam (Pfizer Inc.). The skull flap was repositioned and secured with cyanoacrylate (Vetbond; 3M), and the skin was sutured. The marmosets were placed in a humidicrib until recovery of movement, after which they were returned to the mothers (infant animals) and, in all cases, subsequently reintroduced to the colony. Postoperative analgesic (oral meloxicam 0.005 mg/kg for neonates, 0.05 mg/kg for adults, 3 d) and antibiotic (oral cephalexin 30 mg/kg, 5 d) were administered.

Throughout the postlesion period, the marmosets were housed in large cages with family groups having access to both indoor and outdoor environments. All animals demonstrated normal patterns of movement, including the capacity to perform fine grasping and holding movements and to perform precise jumps across tree branches, and did not require assistance for daily activities such as seeking and obtaining food.

Fluorescent Tracer Injections. Following long survival times (Table 1), the animals were premedicated with i.m. injections of diazepam (3.0 mg/kg) and atropine (0.2 mg/kg) and anesthetized with ketamine (50 mg/kg) and xylazine (3 mg/kg). They were placed in a stereotaxic frame, and the cortex was exposed. The retrograde fluorescent tracers DY (2% in dH_2O) and FB (2% in dH_2O) were injected using 1-μL syringes fitted with glass micropipettes inserted through small cuts in the dura mater. These injections (*SI Appendix*, Fig. S2) typically covered all cortical layers. Visualization of the caudal tip of the lateral sulcus and stereotaxic coordinates obtained in the course of previous studies (65, 67) guided the placement of the injections (their exact location in relation to cortical areas was assessed post mortem by examination of myelin-stained sections; *SI Appendix*, Fig. S2). The cortex was covered with Gelfilm, the piece of bone removed during the craniotomy was fixed back in place with dental acrylic, and the wound was sutured. Analgesics (oral paracetamol, three drops every 6 h) and antibiotics (Norocillin, 0.1 mL) were given for the first 24 h postsurgery. The animals were returned to their home cages for a period of 2 wk before euthanasia and perfusion.

Tissue Processing and Fluorescence Immunohistochemistry. At the conclusion of experiments, the marmosets were overdosed with pentobarbitone sodium (100 mg/kg) and transcardially perfused with 0.1 M heparinized phosphate buffer (PB; pH 7.2) followed by 4% paraformaldehyde (PFA) in 0.1 M PB. The

Table 1. Details of sex, age, lesion, and tracer injections in all subjects

Subject (Sex)	Age at lesion	Age at perfusion (months)	Survival time (months)	Number of tracer-labeled neurons in LGN	Analyzed LGN	LGN volume loss (%)
W6F(M)	38 d	17	16	55 (FB)	both	38.04
W6G(F)	43 d	25	24	#	both	33.80
W6H(M)	42 d	21	20	#	both	40.16
W6I(M)	42 d	29	28	68(FB)	left	46.71
W6J(F)	42 d	24	23	7(FB), 18(DY)	both	32.69
W6K(M)	46 d	33	31	46 (FB)	left	27.03
W6L*(F)	46 d	35	33	21(FB)	left	41.25
WA9(M)	18 mo	57	38	#	both	46.30
WA11(M)	23 mo	44	21	#	left	45.08
WA13(M)	28 mo	56	28	27(FB), 11(DY)	both	28.74
WA14(F)	25 mo	55	30	42 (FB)	left	47.91
WA15(F)	25 mo	37	11	53(FB), 13(DY)	both	56.61
WA17*(M)	31 mo	56	23	30(FB)	left	31.57
WA18*(F)	24 mo	48	23	59(FB)	left	44.27
CJ183(M)	—	34	—	#	left	—
CJ185(F)	—	35	—	#	left	—
CJ187(F)	—	31	—	2(FB)	right	—
CJ200(F)	—	43	—	3(FB)	right	—
CJ206(F)	—	67	—	46(FB)	right	—
CJ207(F)	—	67	—	22(FB)	right	—

Lesion was in the left hemisphere for all cases. # indicates no tracer injection.
*Represents animals that were not used in immunohistochemistry experiments.

brains were dissected and postfixed in the same medium for 24 h followed by immersion in buffered 4% PFA solutions containing increasing concentrations of sucrose (10%, 20%, and 30%). Frozen 40-μm coronal sections were obtained using a cryostat in five series devoted to different immunostaining procedures and myelin staining. In the animals that received tracers, one unstained series was used for analysis of connections.

For fluorescence immunostaining, the sections were incubated in blocking solution (10% normal horse serum and 0.3% Triton-X100 in 0.1 M PB) for 1 h at room temperature and then incubated with the primary antibody for CB-D28K (goat polyclonal [PA5-469361, 1:50] from Thermo Fisher Scientific or mouse monoclonal from Swant, Code 300, 1:5,000), PV (from Swant, either mouse monoclonal [Code 235, 1:1,000] or rabbit anti-PV [Code PV 27, 1:5,000]), and NeuN (1:800, Merck Millipore, MAB377, Clone A60) at 4 °C for 42 to 46 h. Secondary antibodies (1:600, Abcam; donkey anti-mouse IgG H&L [ab150109], donkey anti-goat IgG H&L [ab150135] and donkey anti-rabbit IgG H&L [ab150064]) were applied for 60 min at room temperature. For PV and CB immunohistochemistry, two choices of antibodies that were raised in different species produced similar results both in the neocortex and LGN (*SI Appendix*, Fig. S6).

Quantification and Statistical Analysis.

LGN volume measurement. NeuN-stained sections containing the LGN were scanned using the Aperio Scanscope AT Turbo (Leica Biosystems) at 20× magnification as detailed previously (4). Briefly, an estimate of the volume of the LGN was obtained using the Cavalieri estimator based on the area measured in serial sections through this nucleus. The total volume of the LGN was calculated based on the sum of the volumes obtained for each section and corrected for a shrinkage factor of 0.801 (4, 5).

Mapping of retrogradely labeled neurons. The sections in the unstained series were examined using a Zeiss Axioplan fluorescence microscope, and labeled cell bodies were plotted with an X-Y stage digitizer (MD-3, Accustage) and associated software (MD-Plot, version 5.3). The entire cortex and thalamic nuclei were examined for fluorescent cell bodies. Digital files containing the position of each labeled neuron, together with the outlines of the injection sites, the inner and outer boundaries of the cortex, and other anatomical landmarks, were imported into Adobe Illustrator, which was used to align the locations of labeled cells with images of the cortical cytoarchitecture. These images were used to quantify the numbers of labeled neurons in each cytoarchitectural area using built-in functions of Adobe Illustrator. The percentages of LGN-labeled neurons in each case were normalized to the number of neurons labeled in intralaminar thalamic nuclei to account for variability of tracer's injections (Fig. 8C).

Colocalization assessment. Using sections in the immunostained series, the LGN images were captured and tiled using a Nikon C1 laser scanning confocal microscope at 20× magnification. The same fields of LGN were imaged with excitation filters suited to the 488-, 594-, 647-, and 405-nm laser lines to capture all fluorescent tags present. ImageJ software was used for analysis of confocal images.

For analysis of CB expression in M and P neurons (Fig. 5), we manually counted and marked all PV-immunoreactive neurons with clear staining within the M and P layers of the nondegenerated part of LGN regardless of staining intensity. Three consecutive coronal LGN sections (at least 120 μm apart) obtained from the central portion of the LGN [interaural level +4.8 to +5.15 mm (33)], accounting for at least 1,000 PV-expressing neurons, were used. We then counted CB-expressing neurons from the population of labeled neurons and calculated the percentage of double-labeled neurons. While the pattern of coexpression was the same in all animals of each group, for this analysis, the three animals with the best staining were chosen from each group. We similarly counted neurons coexpressing CB and PV from the population of CB-expressing neurons in the degenerated zone (Fig. 6B). For this purpose, every LGN section that contained a degenerated zone was used. The numbers of CB-expressing neurons in the LPZ were expressed as the percentage of all surviving neurons, labeled by NeuN (Fig. 6C).

For mapping of colocalization of neuronal tracers (FB or DY) with CB and PV, we not only used tiled images but also imaged separately each single traced neuron at all relevant excitation wavelengths to best understand its expression profile. For some neurons, Z-stack images (with step size of 5 μm) were required to best identify the expression profile.

Statistics. Differences were assessed using one- or two-way ANOVA followed by post hoc Tukey's tests. The Student's t test was only used for comparison of the two groups presented in Fig. 6 B and C. The correlation analysis was used for data in Figs. 5 D and E and 8D. Results presented here are displayed as the mean ± SEM (SEM). Significance was set at $P < 0.05$.

1. J. C. Horton, W. F. Hoyt, The representation of the visual field in human striate cortex. A revision of the classic Holmes map. *Arch. Ophthalmol.* **109**, 816–824 (1991).
2. J. M. Vanburen, Trans-synaptic retrograde degeneration in the visual system of primates. *J. Neurol. Neurosurg. Psychiatry* **26**, 402–409 (1963).
3. A. Cowey, P. Stoerig, Projection patterns of surviving neurons in the dorsal lateral geniculate nucleus following discrete lesions of striate cortex: Implications for residual vision. *Exp. Brain Res.* **75**, 631–638 (1989).
4. N. Atapour, K. H. Worthy, L. L. Lui, H. H. Yu, M. G. P. Rosa, Neuronal degeneration in the dorsal lateral geniculate nucleus following lesions of primary visual cortex: Comparison of young adult and geriatric marmoset monkeys. *Brain Struct. Funct.* **222**, 3283–3293 (2017).
5. N. Atapour, K. H. Worthy, M. G. P. Rosa, Neurochemical changes in the primate lateral geniculate nucleus following lesions of striate cortex in infancy and adulthood: Implications for residual vision and blindsight. *Brain Struct. Funct.* **226**, 2763–2775 (2021).
6. H. H. Yu, N. Atapour, T. A. Chaplin, K. H. Worthy, M. G. P. Rosa, Robust visual responses and normal retinotopy in primate lateral geniculate nucleus following long-term lesions of striate cortex. *J. Neurosci.* **38**, 3955–3970 (2018).
7. Z. F. Kisvárday, A. Cowey, P. Stoerig, P. Somogyi, Direct and indirect retinal input into degenerated dorsal lateral geniculate nucleus after striate cortical removal in monkey: Implications for residual vision. *Exp. Brain Res.* **86**, 271–292 (1991).
8. M. Yukie, E. Iwai, Direct projection from the dorsal lateral geniculate nucleus to the prestriate cortex in macaque monkeys. *J. Comp. Neurol.* **201**, 81–97 (1981).
9. C. E. Warner et al., Preservation of vision by the pulvinar following early-life primary visual cortex lesions. *Curr. Biol.* **25**, 424–434 (2015).
10. L. Weiskrantz, *Blindsight: A Case Study and Implications* (Oxford University Press, Oxford, 1986).
11. M. C. Schmid et al., Blindsight depends on the lateral geniculate nucleus. *Nature* **466**, 373–377 (2010).
12. S. Ajina, H. Bridge, Blindsight relies on a functional connection between hMT+ and the lateral geniculate nucleus, not the pulvinar. *PLoS Biol.* **16**, e2005769 (2018).
13. S. Ajina, G. Rees, C. Kennard, H. Bridge, Abnormal contrast responses in the extrastriate cortex of blindsight patients. *J. Neurosci.* **35**, 8201–8213 (2015).
14. R. Dubner, S. M. Zeki, Response properties and receptive fields of cells in an anatomically defined region of the superior temporal sulcus in the monkey. *Brain Res.* **35**, 528–532 (1971).
15. R. T. Born, D. C. Bradley, Structure and function of visual area MT. *Annu. Rev. Neurosci.* **28**, 157–189 (2005).
16. T. A. Chaplin et al., Sensitivity of neurons in the middle temporal area of marmoset monkeys to random dot motion. *J. Neurophysiol.* **118**, 1567–1580 (2017).
17. H. R. Rodman, C. G. Gross, T. D. Albright, Afferent basis of visual response properties in area MT of the macaque. II. Effects of superior colliculus removal. *J. Neurosci.* **10**, 1154–1164 (1990).
18. H. Bridge, O. Thomas, S. Jbabdi, A. Cowey, Changes in connectivity after visual cortical brain damage underlie altered visual function. *Brain* **131**, 1433–1444 (2008).
19. K. R. Huxlin et al., Perceptual relearning of complex visual motion after V1 damage in humans. *J. Neurosci.* **29**, 3981–3991 (2009).
20. S. H. Hendry, T. Yoshioka, A neurochemically distinct third channel in the macaque dorsal lateral geniculate nucleus. *Science* **264**, 575–577 (1994).
21. Y. H. Yan, A. Winarto, I. Mansjoer, A. Hendrickson, Parvalbumin, calbindin, and calretinin mark distinct pathways during development of monkey dorsal lateral geniculate nucleus. *J. Neurobiol.* **31**, 189–209 (1996).
22. A. K. Goodchild, P. R. Martin, The distribution of calcium-binding proteins in the lateral geniculate nucleus and visual cortex of a New World monkey, the marmoset, Callithrix jacchus. *Vis. Neurosci.* **15**, 625–642 (1998).
23. L. C. Sincich, K. F. Park, M. J. Wohlgemuth, J. C. Horton, Bypassing V1: A direct geniculate input to area MT. *Nat. Neurosci.* **7**, 1123–1128 (2004).
24. S. H. Hendry, R. C. Reid, The koniocellular pathway in primate vision. *Annu. Rev. Neurosci.* **23**, 127–153 (2000).
25. C. Vakalopoulos, A theory of blindsight–The anatomy of the unconscious: A proposal for the koniocellular projections and intralaminar thalamus. *Med. Hypotheses* **65**, 1183–1190 (2005).
26. M. A. Hagan, T. A. Chaplin, K. R. Huxlin, M. G. P. Rosa, L. L. Lui, Altered sensitivity to motion of area MT neurons following long-term V1 lesions. *Cereb. Cortex* **30**, 451–464 (2020).
27. H. H. Yu et al., Visually evoked responses in extrastriate area MT after lesions of striate cortex in early life. *J. Neurosci.* **33**, 12479–12489 (2013).

Atapour et al.
Remodeling of lateral geniculate nucleus projections to extrastriate area MT following long-term lesions of striate cortex

PNAS | 9 of 10
https://doi.org/10.1073/pnas.2117137119

28. E. L. Saionz, D. Tadin, M. D. Melnick, K. R. Huxlin, Functional preservation and enhanced capacity for visual restoration in subacute occipital stroke. *Brain* **143**, 1857–1872 (2020).

29. L. T. Mihailović, D. Cupić, N. Dekleva, Changes in the numbers of neurons and glial cells in the lateral geniculate nucleus of the monkey during retrograde cell degeneration. *J. Comp. Neurol.* **142**, 223–229 (1971).

30. C. E. Warner, Y. Goldshmit, J. A. Bourne, Retinal afferents synapse with relay cells targeting the middle temporal area in the pulvinar and lateral geniculate nuclei. *Front. Neuroanat.* **4**, 8 (2010).

31. J. J. Nassi, E. M. Callaway, Multiple circuits relaying primate parallel visual pathways to the middle temporal area. *J. Neurosci.* **26**, 12789–12798 (2006).

32. I. Stepniewska, H. X. Qi, J. H. Kaas, Do superior colliculus projection zones in the inferior pulvinar project to MT in primates? *Eur. J. Neurosci.* **11**, 469–480 (1999).

33. G. Paxinos, C. Watson, M. Petrides, M. G. P. Rosa, H. Tokuno, *The Marmoset Brain in Stereotaxic Coordinates* (Academic, Amsterdam, London, 2012).

34. S. G. Solomon, Striate cortex in dichromatic and trichromatic marmosets: Neurochemical compartmentalization and geniculate input. *J. Comp. Neurol.* **450**, 366–381 (2002).

35. G. N. Elston, M. G. P. Rosa, Morphological variation of layer III pyramidal neurones in the occipitotemporal pathway of the macaque monkey visual cortex. *Cereb. Cortex* **8**, 278–294 (1998).

36. S. M. Palmer, M. G. P. Rosa, Quantitative analysis of the corticocortical projections to the middle temporal area in the marmoset monkey: Evolutionary and functional implications. *Cereb. Cortex* **16**, 1361–1375 (2006).

37. S. Zeki, D. H. Ffytche, The Riddoch syndrome: Insights into the neurobiology of conscious vision. *Brain* **121**, 25–45 (1998).

38. I. T. Diamond, D. Fitzpatrick, D. Schmechel, Calcium binding proteins distinguish large and small cells of the ventral posterior and lateral geniculate nuclei of the prosimian galago and the tree shrew (Tupaia belangeri). *Proc. Natl. Acad. Sci. U.S.A.* **90**, 1425–1429 (1993).

39. M. Kinoshita *et al.*, Dissecting the circuit for blindsight to reveal the critical role of pulvinar and superior colliculus. *Nat. Commun.* **10**, 135 (2019).

40. R. Kato, K. Takaura, T. Ikeda, M. Yoshida, T. Isa, Contribution of the retino-tectal pathway to visually guided saccades after lesion of the primary visual cortex in monkeys. *Eur. J. Neurosci.* **33**, 1952–1960 (2011).

41. M. Tamietto *et al.*, Collicular vision guides nonconscious behavior. *J. Cogn. Neurosci.* **22**, 888–902 (2010).

42. L. Georgy, A. Celeghin, C. A. Marzi, M. Tamietto, A. Ptito, The superior colliculus is sensitive to gestalt-like stimulus configuration in hemispherectomy patients. *Cortex* **81**, 151–161 (2016).

43. N. Takakuwa, K. Isa, H. Onoe, J. Takahashi, T. Isa, Contribution of the pulvinar and lateral geniculate nucleus to the control of visually guided saccades in blindsight monkeys. *J. Neurosci.* **41**, 1755–1768 (2021).

44. L. Georgy, B. Jans, M. Tamietto, A. Ptito, Functional reorganization of population receptive fields in a hemispherectomy patient with blindsight. *Neuropsychologia* **128**, 198–203 (2019).

45. J. E. Hsu, T. A. Jones, Contralesional neural plasticity and functional changes in the less-affected forelimb after large and small cortical infarcts in rats. *Exp. Neurol.* **201**, 479–494 (2006).

46. W. S. Choi, E. Lee, J. Lim, Y. J. Oh, Calbindin-D28K prevents drug-induced dopaminergic neuronal death by inhibiting caspase and calpain activity. *Biochem. Biophys. Res. Commun.* **371**, 127–131 (2008).

47. I. G. Dopeso-Reyes *et al.*, Calbindin content and differential vulnerability of midbrain efferent dopaminergic neurons in macaques. *Front. Neuroanat.* **8**, 146 (2014).

48. D. C. German, K. F. Manaye, P. K. Sonsalla, B. A. Brooks, Midbrain dopaminergic cell loss in Parkinson's disease and MPTP-induced parkinsonism: Sparing of calbindin-D28k-containing cells. *Ann. N. Y. Acad. Sci.* **648**, 42–62 (1992).

49. T. Yamada, P. L. McGeer, K. G. Baimbridge, E. G. McGeer, Relative sparing in Parkinson's disease of substantia nigra dopamine neurons containing calbindin-D28K. *Brain Res.* **526**, 303–307 (1990).

50. S. Y. Kook *et al.*, Crucial role of calbindin-D28k in the pathogenesis of Alzheimer's disease mouse model. *Cell Death Differ.* **21**, 1575–1587 (2014).

51. J. H. Kim *et al.*, Overexpression of calbindin-D28K in hippocampal progenitor cells increases neuronal differentiation and neurite outgrowth. *FASEB J.* **20**, 109–111 (2006).

52. D. Gonzalez *et al.*, Effects of monocular enucleation on calbindin-D 28k and c-Fos expression in the lateral geniculate nucleus in rats. *Okajimas Folia Anat. Jpn.* **82**, 9–18 (2005).

53. A. Cowey, P. Stoerig, V. H. Perry, Transneuronal retrograde degeneration of retinal ganglion cells after damage to striate cortex in macaque monkeys: Selective loss of P beta cells. *Neuroscience* **29**, 65–80 (1989).

54. J. Dineen, A. Hendrickson, E. G. Keating, Alterations of retinal inputs following striate cortex removal in adult monkey. *Exp. Brain Res.* **47**, 446–456 (1982).

55. A. Hendrickson *et al.*, Retrograde transneuronal degeneration in the retina and lateral geniculate nucleus of the V1-lesioned marmoset monkey. *Brain Struct. Funct.* **220**, 351–360 (2015).

56. R. E. Weller, J. H. Kaas, Parameters affecting the loss of ganglion cells of the retina following ablations of striate cortex in primates. *Vis. Neurosci.* **3**, 327–349 (1989).

57. L. L. Lui, M. G. P. Rosa, Structure and function of the middle temporal visual area (MT) in the marmoset: Comparisons with the macaque monkey. *Neurosci. Res.* **93**, 62–71 (2015).

58. C. Meissirel, K. C. Wikler, L. M. Chalupa, P. Rakic, Early divergence of magnocellular and parvocellular functional subsystems in the embryonic primate visual system. *Proc. Natl. Acad. Sci. U.S.A.* **94**, 5900–5905 (1997).

59. J. M. Chan, K. H. Worthy, M. G. P. Rosa, D. H. Reser, N. Atapour, Volume reduction without neuronal loss in the primate pulvinar complex following striate cortex lesions. *Brain Struct. Funct.* **226**, 2417–2430 (2021).

60. N. Dancause *et al.*, Extensive cortical rewiring after brain injury. *J. Neurosci.* **25**, 10167–10179 (2005).

61. C. Darian-Smith, C. D. Gilbert, Axonal sprouting accompanies functional reorganization in adult cat striate cortex. *Nature* **368**, 737–740 (1994).

62. P. M. Abdul-Muneer, B. J. Pfister, J. Haorah, N. Chandra, Role of matrix metalloproteinases in the pathogenesis of traumatic brain injury. *Mol. Neurobiol.* **53**, 6106–6123 (2016).

63. N. George, H. M. Geller, Extracellular matrix and traumatic brain injury. *J. Neurosci. Res.* **96**, 573–588 (2018).

64. A. Represa, Y. Ben-Ari, Trophic actions of GABA on neuronal development. *Trends Neurosci.* **28**, 278–283 (2005).

65. M. G. P. Rosa, R. Tweedale, G. N. Elston, Visual responses of neurons in the middle temporal area of New World monkeys after lesions of striate cortex. *J. Neurosci.* **20**, 5552–5563 (2000).

66. T. A. Chaplin, H. H. Yu, M. G. P. Rosa, Representation of the visual field in the primary visual area of the marmoset monkey: Magnification factors, point-image size, and proportionality to retinal ganglion cell density. *J. Comp. Neurol.* **521**, 1001–1019 (2013).

67. M. G. P. Rosa, G. N. Elston, Visuotopic organisation and neuronal response selectivity for direction of motion in visual areas of the caudal temporal lobe of the marmoset monkey (Callithrix jacchus): Middle temporal area, middle temporal crescent, and surrounding cortex. *J. Comp. Neurol.* **393**, 505–527 (1998).